ISSN (Print) 1226-1750
ISSN (Online) 2233-6656
Journal of Magnetics 25(1), 86-91 (2020) https://doi.org/10.4283/JMAG.2020.25.1.086

Analytical Calculation of Resistance, Leakage Inductance and Parasitic Capacitance for High Frequency Transformer

Young-Un Park[1], Hwan-Su Lee[2], and Dae-kyong Kim[3]*

[1]*Green Energy Institute, Korea*
[2]*ENITT, Naju-si, Korea*
[3]*Dept. of Electrical Engineering, Sunchon National University, Korea*

(Received 9 January 2020, Received in final form 17 February 2020, Accepted 19 February 2020)

The design of a high-frequency transformer, which is the main component of a DC/DC converter, is very important. In the case of a DC transmission system, such as HVDC, the transformer should use high power and high frequency, but there are few studies in this category. Therefore, this study examined the design of a high frequency transformer. When designing the transformer covered in this paper, it is necessary to consider the frequency components differently from a traditional transformer design. Therefore, winding resistance, leakage inductance, and parasitic capacitance were calculated according to the frequency change, and finite element method (FEM) analysis and comparative analysis were conducted for validation.

Keywords : AC resistance, high frequency transformer, leakage inductance, parasitic capacitance

1. Introduction

Considerable efforts have been made to improve the performance of power systems. In particular, the emphasis is on the power density, efficiency, and reduced passive elements in the inverter. A common method to reduce the size of passive elements is to increase the switching frequency of the inverter [1]. The development of digital home appliances and renewable energy sources has led to increased interest in DC-based transmission and distribution. Commonly used systems are based on alternating current. Therefore, the DC power generated from a renewable energy source is converted to AC power and then converted to another DC power for use in the chosen digital device. DC distribution reduces the unnecessary power conversion steps and improves the power distribution efficiency. On the other hand, in the case of direct current distribution, conversion from DC to a set DC voltage level is required. The DC/DC converter for distribution plays an important role in achieving high efficiency in this process. The design of a high-frequency transformer, which is the main component of a DC/DC converter, is very important [2].

New technology is pushing the switching frequency into the megahertz range to minimize the size of the inductive components, making switching loss more severe. Therefore, an accurate prediction of the leakage inductance, resistance and parasitic capacitance at high frequency is needed to implement an optimized design. The leakage inductance, which is an inductive component of a transformer in power equipment, causes electromagnetic interference and affects the switching loss and reliability [3].

Indeed, leakage inductance reduction with increasing frequency is observed in the measurements. This is mainly because the current distribution within the conductors changes as the frequency increases. At high frequency, the current tends to concentrate on the surface of the conductors and the leakage energy is effectively stored in a narrow cross-sectional area. The total current is not changed. Hence, the leakage inductance is reduced at high frequency. Predictions of the leakage inductance are often used in simulations, which is time consuming [3-6].

Increasing the frequency also increases winding losses due to skin effect and proximity effect. Therefore, a study for accurate calculation of resistance at high frequency is conducted [7].

Also in the case of capacitance, procedures for calculating the capacitance have been proposed for inductors [8], planar transformers [9], magnetic components within SMPS [10], high-frequency transformers [11] and power transformers [12]. A resonant dc-to-dc converter, using

*Corresponding author: Tel: +82-10-4576-0486
Fax: +82-61-750-3540, e-mail: dkkim@sunchon.ac.kr

the high frequency, the parasitic parameters, in particular the self-capacitance, can heavily affect the performance of the converter [13]. This capacitance is responsible for unwanted resonances and oscillations of the primary and secondary side currents, hence reducing the system's efficiency and reliability [14].

Therefore, a precision system needs a technique to calculate more accurate RLC values required. As a result, the efficiency of the system can be improved. For high frequency transformers, more accurate designs are likely to considering AC resistance, leakage inductance and parasitic capacitance.

In this paper, the resistance, leakage inductance and parasitic capacitance for high frequency transformer design is calculated. Analytical methods were used to obtain faster results than finite element analysis.

2. Analysis of Transformer

2.1. Structure and specification of transformer

Figure 1 presents the shape and main dimensions of the 100 kVA high frequency transformer model discussed in this paper. The transformer was a shell type transformer. The size of the core was selected according to the spatial constraints of the system. The magnetic path was determined by considering the magnetic saturation. In addition, the winding of the material, thickness and number of turns was determined considering the current density and voltage ratio. An analysis of the characteristics of the transformer through the equivalent circuit requires that resistance, inductance, and capacitance be considered so that accurate nuclear stones can be obtained. The equivalent circuit can be designed, as shown in Fig. 2.

2.2. Wire resistance [6]

The resistance of a winding can be calculated usually as in equation (1) when winding material is copper.

$$R_{dc} = \frac{\rho l}{S},\ \rho = \rho_0 \times (1 + 0.00393 \times t) \tag{1}$$

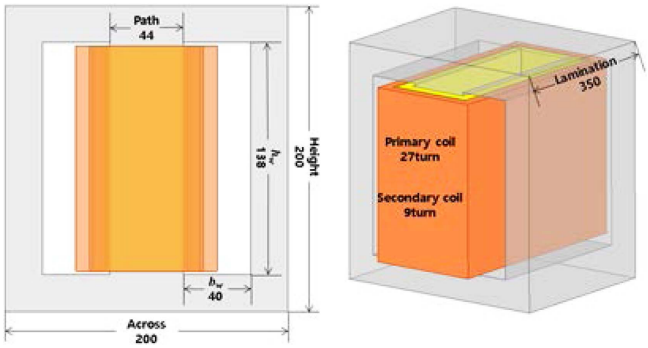

Fig. 1. (Color online) Transformer shape and main dimensions.

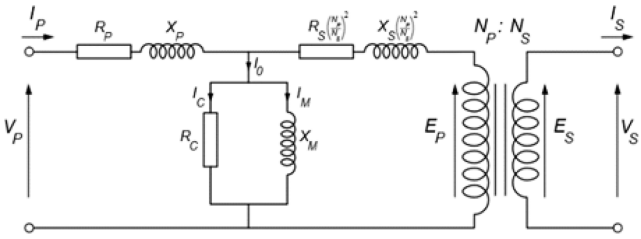

Fig. 2. Equivalent circuit of transformer.

Where, ρ is the resistivity, S is the conductor cross sectional area, l is the winding length, R is the DC resistance. Also, ρ_0 is the resistivity in the 0 °C, t is the winding temperature. However, as the frequency increases, the effect of the skin effect increases, and the proximity effect occurs because the coil is close to several turns. In order to reduce the effect of the skin effect and the proximity effect, the windings of high-frequency transformer adopt the Litz-wire. Fig. 3 shows the current density of the windings with skin depth and proximity effect. Therefore, the winding resistance at high frequency can be expressed as equation (5) [6].

$$R_{ac} = F_r \times R_{dc} \tag{2}$$

$$F_r = y \times \left[M(y) + \frac{2}{3} \times (m^2 - 1) \times D(y) \right] \tag{3}$$

$$y = \frac{h_c}{\delta},\ \delta = \frac{1}{\sqrt{\pi f \mu_{copper} \gamma}} = \frac{0.0671}{\sqrt{f}},$$
$$h_c = 0.834 \times d \times Sq[\mathrm{d/s}],\ S_q = n \times \pi \times r^2 \tag{4}$$

$$M(y) = \frac{\sin h(2y) + \sin(2y)}{\cos h(2y) - \cos(2y)},$$
$$D(y) = \frac{\sin h(y) - \sin(y)}{\cos h(2y) + \cos(2y)} \tag{5}$$

Where m is number of winding layers, δ is skin depth, R_{dc} is DC resistance, F_r is AC-to-DC winding resistance ratio, d is the wire diameter, Sq is square of coil, and R_{ac} is AC resistance. Figure 3 shows the calculation results of the winding resistances on the primary and secondary of the transformer. The conductivity of copper at room temperature is 5.618×10^7 s/m, the magnetic permeability of copper (μ_{copper}) is $4 \times \pi \times 10^{-7}$ H/m.

2.3. Leakage inductance

AC current in the primary winding of the transformer and all magnetic flux produced by it is routed along the magnetic core and connected to the secondary winding. Some magnetic flux leaks to the air winding layer insulation layer because the flux linkage between the two windings is not perfect, as shown in Fig. 1. If the secondary

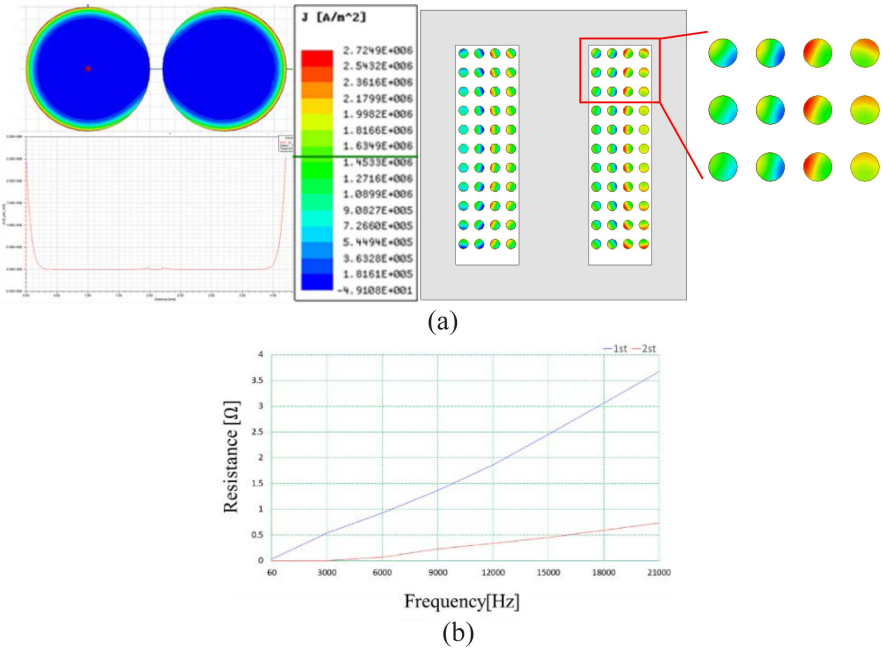

Fig. 3. (Color online) Current density distribution and resistance of windings due to proximity effect. (a) The winding current density due to skin effect and proximity effect, (b) Winding resistance due to frequency varying.

is short-circuited, the main flux in the core that links both windings will be negligible because the primary and secondary ampere turns almost cancel. This means the leakage energy. If the permeability is infinite ($\mu_r \rightarrow \infty$, $\sigma \rightarrow 0$), the magnetic field strength is zero inside the core. Usually, the core window height, h_w, is longer than the core window width, b_w as shown Fig. 1. Therefore, the end effect can be ignored, and the leakage flux is almost parallel to the interface between the conductive layers. The current is concentrated at the surface of the conductor at a high frequency and has the effect of reducing the conductor cross-sectional area, which equivalently stores the leakage energy. That is, the leakage inductance decreases with increasing frequency. Because of the eddy current effect, the current is no longer distributed evenly within the conductor at high frequency, as shown in Fig. 4. The area of the magneto motive force (MMF) curve is smaller than the low frequency MMF because the leakage energy stored at the high frequency is small.

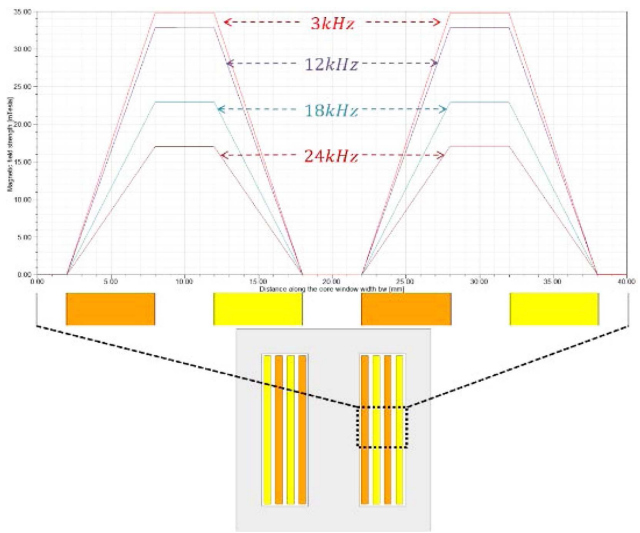

Fig. 4. (Color online) Variation of MMF at high frequency.

The Maxwell's equations for a linear homogeneous isotropic medium in a magnetoquasistatic system are as follows: [2]

$$\nabla \times E = -\mu_0 \cdot \frac{\partial H}{\partial t} \tag{6}$$

$$\nabla \times H = \sigma \cdot E \tag{7}$$

The Cartesian coordinate system is used to solve the Maxwell's equations. The coordinate components of the electric field strength, E, and the magnetic field strength, H, inside the conductor satisfy the following identity by symmetry, as shown in Fig. 5.

$$E_x = 0,\ E_z = 0,\ \frac{\partial E_y}{\partial z} = 0 \tag{8}$$

$$H_x = 0,\ H_z = 0,\ \frac{\partial H_z}{\partial y} = 0 \tag{9}$$

The electric field strength, E, and the magnetic field strength, H, have only the y component and z component, respectively. E and H are functions of z because the two

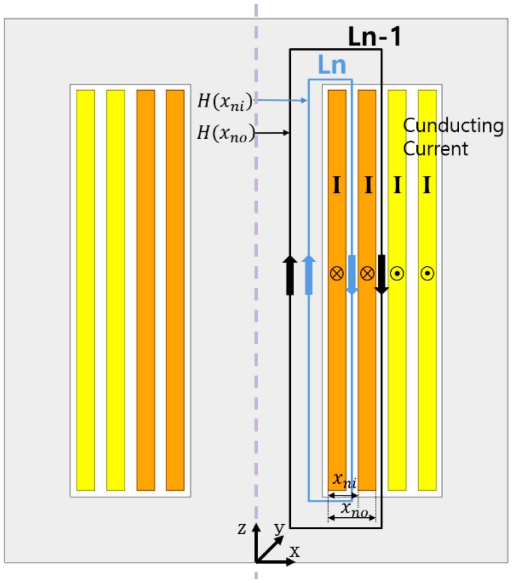

Fig. 5. (Color online) Magnetic field of inner and outer boundary at the *n*-th layer.

fields do not diverge inside the conductor. Therefore, the Maxwell's equations in the phasor are as follows:

$$\frac{dE_y}{dx} = -j\omega\mu_0 H_z \tag{10}$$

$$-\frac{\partial H_z}{\partial x} = -\sigma \cdot E_y \tag{11}$$

When the expression for a given E_y was introduced into Eq. (10) by referring to expression (11), the Helmholtz differential equation is as follows:

$$\frac{d^2 H_z}{dx^2} = -j\omega\mu_0 H_z \tag{12}$$

Owing to the magnetic field strength, H only has a z-component, so the subscripts will drop. The general solution of the Helmholtz equation is as follows:

$$H(x) = H_1 e^{\gamma x} + H_2 e^{-\gamma x} \tag{13}$$

H_1 and H_2 are determined by the complex constant, and the boundary conditions are

$$\gamma = \sqrt{j\omega\mu_0\sigma} = \frac{1+j}{\delta_\omega} \tag{14}$$

where δ_w is the skin depth and $\delta_\omega = \dfrac{1}{\sqrt{\pi f \mu_0 \sigma}}$.

As shown in Eqs. (15) and (16), Ampere's law was applied for closed loops, L_n and L_{n-1} in Fig. 5. The internal and external boundary conditions for the nth layer of the primary winding were obtained within the high permeability ($\mu_r \to \infty$, $\sigma \to 0$). The magnetic field strength for the nth layer of the secondary winding section can be calculated in the same manner but using the reverse of the internal and external boundary conditions because the magnetic field strength falls to zero in the secondary section in the same way.

$$H(x_{ni}) = (n-1)H_0 \tag{15}$$

$$H(x_{no}) = nH_0 \tag{16}$$

Where

$$H_0 = \frac{mI}{h_w} \tag{17}$$

x_{ni} and x_{no} are the distance from the internal surface of the first conductor to the outer surface of the nth floor. m is the number of wires that rotate on each layer, and each wire carries a constant current. When applying boundary conditions (10) and (11) to the Helmholtz Eq. (8), the following constants are obtained:

$$H_1 = H_0 \frac{ne^{\gamma x_{ni}} - (n-1)e^{\gamma x_o}}{2\sinh(\gamma t)} \tag{18}$$

$$H_2 = H_0 \frac{(n-1)e^{\gamma x_o} - ne^{\gamma x_{ni}}}{2\sinh(\gamma t)} \tag{19}$$

where $t = x_{no} - x_{ni}$ is the conductor thickness. The magnetic field strength inside the nth layer along the layer thickness obtained by substituting (18) and (19) for (13) can be expressed as follows:

$$H(x) = H_0 \frac{n\sinh(\gamma x) + (n-1)\sinh(\gamma t - \gamma x)}{2\sinh(\gamma t)} \tag{20}$$

Where x starts at the beginning of the n-th layer to do the simplified calculation in the next step. x does not start at the beginning of the first layer. This means that $x = 0$ in (15) is equal to $x = x_{ni}$ (refers to (18)) in the preceding expression. $lw \cdot hw \cdot dx$ is the the differential volume of the layer element dx. Therefore, the stored energy of each layer is

$$E_i = \frac{1}{2}\mu_0 l_w h_w \int_0^t H(x)^2 \cdot dx \tag{21}$$

where l_w is the mean turn length. Applying (20) to (21), the energy stored in the primary winding can be obtained by substituting (15) into (16) as follows:

$$E_p = \sum_{i=1}^{n_p} E_i = \frac{\mu_0 l_w h_w n_p H_{0p}^2 [k_1(2n_p^2+1) + 4k_2(n_p^2-1)]}{24\gamma \sinh^2(\gamma t_p)} \tag{22}$$

Where

$$k_1 = \sinh(2\gamma t_p) = 2\gamma t_p \tag{23}$$

$$k_2 = \gamma t_p \cosh(\gamma \cdot t_p) - \sinh(\gamma \cdot t_p) \tag{24}$$

$$H_{0p} = \frac{m_p I_p}{h_w} \tag{25}$$

The energy stored in the secondary applied the same approach is

$$E_s = \sum_{i=1}^{n_s} E_i = \frac{\mu_0 l_w h_w n_p H_{0s}^2 [k_3(2n_s^2+1) + 4k_4(n_s^2-1)]}{24\gamma \sinh^2(\gamma t_s)} \tag{26}$$

Where

$$k_3 = \sinh(2\gamma t_s) = 2\gamma t_s \tag{27}$$

$$k_4 = \gamma t_s \cosh(\gamma \cdot t_s) - \sinh(\gamma \cdot t_s) \tag{28}$$

$$H_{0s} = \frac{m_s I_s}{h_w} \tag{29}$$

Each conductive layer is insulated and can be expressed by the insulation layers. The magnetic field strength is kept constant for each insulation layer, which is equal to the magnetic field strength of the outer surface of each conductor layer. Therefore, the total energy stored in the insulation can be expressed using (30) [2].

$$\begin{aligned} E_{insu} &= \frac{1}{2}\mu_0 l_w h_w \left[\left(\frac{m_p I_p}{hw}\right)^2 t_{iso} \sum_{i=1}^{n_p} i^2 + \left(\frac{m_s I_s}{hw}\right)^2 t_{iso} \sum_{i=1}^{n_s-1} i^2 \right] \\ &= \frac{\mu_0 l_w h_w}{12 h_w} [(m_p I_p)^2 n_p (n+1)(2n_p+1) \\ &\quad + (m_s I_s)^2 n_s (n_s-1)(2n_s-1)] \end{aligned} \tag{30}$$

As the frequency increases, the value of k decreases, so that E_p, and E_s also decrease, as shown in Fig. 6. Where t_{iso} is the thickness of insulation between each of the two layers. The total leakage energy is the sum of the energy stored in each elementary layer and can be expressed as (31).

$$E_{total} = E_p + E_s + E_{insu} = \frac{1}{2} L_{lk} I_p^2 \tag{31}$$

For simplification, an example that has only one turn in each layer ($m_p = m_s = 1$) is given. The p is the turns ratio of n_s and n_p, and $t_p = t_s$ is the thickness of the conductors. Hence, the total leakage inductance referred to the primary side can be expressed using (32).

$$\begin{aligned} L_{lk} = \frac{\mu_0 l_w n_p}{6hw} \Bigg\{ & \frac{n_p^2 (k_1 + 2k_2)(p+1)}{\gamma \sinh^2(\gamma t_p)} + \frac{(k_1 - 4k_2)(p+1)}{2p\gamma \sinh^2(\gamma t_p)} \\ & + \left[2n_p^2 + 2p \cdot n_p^2 + \frac{1}{p} + 1 \right] t_{\text{iso}} \Bigg\} \end{aligned} \tag{32}$$

The AC current in the primary winding of the transformer and all magnetic flux produced by it are routed along the magnetic B_m, and μ_r, which are determined by the core material properties.

Φ_m is calculated using Eq. (2). The core material of transformer used PM7 of TODA ISU company. The LCR meter was used to measure the leakage inductance. That is measured by contacting the LCR Meter probe with the primary winding and shorting the secondary winding as shown in Fig. 7(a). The calculated leakage inductance is closer to the measurement than the FEM simulation, as shown in Fig. 7(b). This confirmed that it had been designed properly.

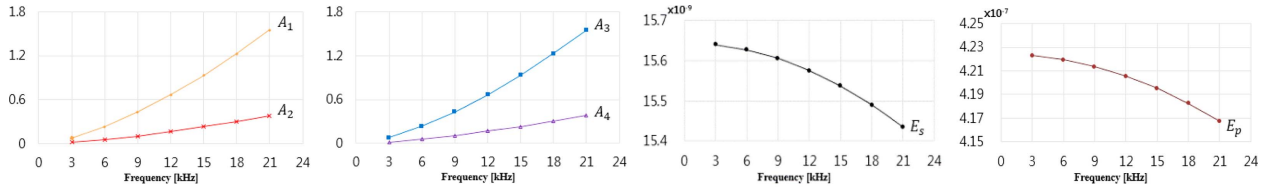

Fig. 6. (Color online) Calculate A1, A2, A3, A4, E_s, E_p.

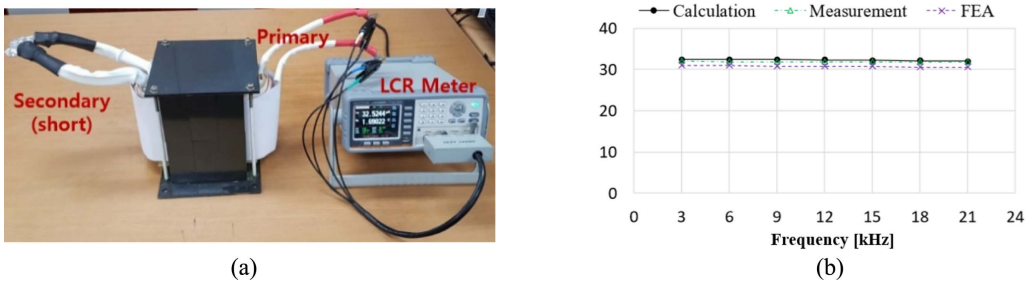

Fig. 7. (Color online) Leakage inductance measurement and results comparison (a) Measurement of leakage inductance (b) Comparison for leakage inductance between calculation, measurement and FEA.

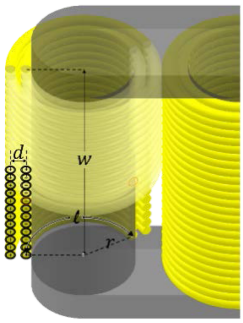

(a)

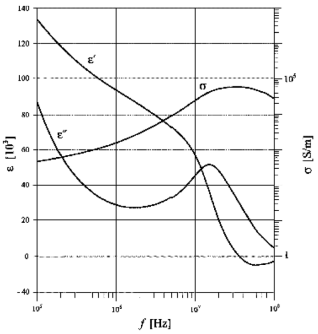

(b)

Item	Calculated [pF]
Self-capacitance of 2nd winding	12.51
Self-capacitance towards screen	46.22
Total self-capacitance	58.73

(c)

Fig. 8. (Color online) Representation of two adjacent layers and parasitic capacitance calculation results (a) two adjacent layers (b) The complex relative permittivity and conductivity for PM7 at 25 °C (c) results of calculated parasitic capacitance.

2.4. Parasitic capacitance

The capacitance is also an element that forms a resonant tank. The parasitic capacitance element between the windings has an influence. Therefore, accurate parasitic capacitance calculations are essential for improving the efficiency of the system. Comprehensive procedures for calculating the parasitic capacitance have been proposed for transformer [7]. Here, the parasitic capacitance can be calculated using Eqs. (34) and (35). Fig. 8(b) shows that the value of ε varies with frequency. Figure 6(c) shows the result of calculating the parasitic capacitance. For the adjacent winding wire an equivalent dielectric constant can be considered, whose expression is the following [14]:

$$\varepsilon_{eqs} = \frac{\varepsilon_w \varepsilon_L (t_w + t_L)}{\varepsilon_L t_w + \varepsilon_L t_L} \tag{33}$$

where ε_{eqs} is the equivalent dielectric constant that accounts for the properties of the insulation of the wires facing the screen and the air between the layer and screen. In addition, t_w and t_L are the dielectric constants of the outer insulation and of the coating of each strand, respectively.

$$C_{II} = \varepsilon_0 \varepsilon_r \frac{2\pi w}{\ln(1 + d/r)} \xrightarrow{r \to \infty} C_{II} = \varepsilon_0 \varepsilon_r \frac{2\pi r w}{d} \tag{34}$$

$$C_{Is} = \sum_{i=1}^{q} \varepsilon_{eqs} \frac{2\pi w}{\ln\left(1 + \frac{ds}{a}\right)} \frac{1}{q^2 z^2} \left(\frac{3z^2 (i-1)^2 + 3z(i-1) + 1}{3} \right) \tag{35}$$

where w is the width of the layer, or the breath of each section. Equation (34) is valid for a large number of turns with axial symmetry. The value of the distance, d, between two wires of different layers plays a decisive role in calculating the capacitance.

3. Conclusions

In this study, a circuit equivalent equation using the resistance, leakage inductance, and parasitic capacitance was applied to calculate the transformer characteristics more accurately considering the frequency. The validity of the proposed equivalent circuit method was confirmed by FEM and comparative analyses. The proposed circuit equivalent method is a useful method for interpreting the fundamental characteristics of high-frequency transformers more efficiently.

Acknowledgements

This work was supported by NRF-2017R1A2B1009684.

References

[1] S.-Y. Kim, Y.-S. Han, and J.-H. Cho, The Korean Institute of Electrical Engineers **10**, 36 (2015).
[2] Ziwei Ouyang and Jun Zhang, IEEE Trans. Power Electron. **30**, 5769 (2015).
[3] Alexander Stadler and Manfred Albach, IEEE Trans. Magn. **42**, 735 (2006).
[4] Xavier Margueron and Jean-Pierre Keradec, IEEE Trans. Ind. Appl. **43**, 884 (2007).
[5] R. Petkov, IEEE Trans. Power. Electron. **11**, 1 (1996).
[6] Lu Zhao, Qiongxuan Ge, Zhida Zhou, Bo Uang, Ke Wang, and Yaohua Li, ICEMS **2018**, 2655 (2018).
[7] A. Massarini and M. K. Kazimierczuk, IEEE Trans. Power Electron. **12**, 671 (1997).
[8] T. Duerbaum and G. Sauerlander, Proc. Appl. Power Electron. Conf. **1**, 109 (2001).
[9] T. Duerbaum, Proc. Power Electron. Spec. Conf. **3**, 1651 (2000).
[10] H. Y. Lu, J. G. Zhu, and S. Y. R. Hui, IEEE Trans. Power Electron. **18**, 1105 (2003).
[11] W. T. Duerdoth, Wireless Eng. **23**, 161 (1946).
[12] F. da Silveira Cavalcante and J. W. Kolar, Proc. Power Electron. Spec. Conf. 1271 (2005).
[13] S. Johnson, A. Witulski, and R. Erickson, IEEE Trans. Aerosp. Electron. Syst. **AES-24**, 263 (1988).
[14] Luca Dalessandro, F. da Silveira Cavalcante, and Johann W. Kolar, IEEE Trans. Power Electron. **22**, 2081 (2007).